High-grade metamorphic rocks from Christmas Point in the Napier Complex, East Antarctica

Yasutaka Yoshimura[1], Tomoharu Miyamoto[2], Edward S. Grew[3], Christopher J. Carson[4], Daniel J. Dunkley[5,*] and Yoichi Motoyoshi[6]

[1]*Department of Natural Environmental Science, Kochi University, Akebono-cho 2-5-1, Kochi 780-8520*
[2]*Department of Earth and Planetary Science, Kyushu University, Hakozaki 6-10-1, Fukuoka 812-8581*
[3]*Department of Geological Science, University of Maine, 5790 Bryand Research Center, Orono, Maine, 04469-5790, U.S.A.*
[4]*Department of Geology and Geophysics, Kline Geology Laboratory, Yale University, 210 Whitney Ave., New Haven, CT 06511, U.S.A.*
[5]*School of Geosciences, Edgeworth David Building, University of Sydney, NSW 2006, Australia*
[6]*National Institute of Polar Research, Kaga 1-chome, Itabashi-ku, Tokyo 173-8515*

Abstract: The Christmas Point area is dominated by well-layered gneisses, of which garnet-orthopyroxene gneiss and garnet felsic gneiss are the most abundant types. Orthopyroxene-bearing quartz-rich granulite, layering of which is indistinct to massive, is present as layers within the garnet felsic gneiss. Garnet-amphibole gneiss is present as layers in both the garnet-orthopyroxene gneiss and the garnet felsic gneiss. Orthopyroxene-bearing quartz-rich granulites contain coexisting orthopyroxene, sillimanite and quartz. The occurrence of sapphirine as inclusions in sillimanite implies that metamorphic conditions changed from the stability field of sapphirine+quartz to that of orthopyroxene+sillimanite+quartz. *P-T* conditions estimated using garnet-orthopyroxene geothermobarometry range from 920 to 1040°C and 8.8 to 11.5 kbar. Garnet exsolution lamellae present in orthopyroxene from the garnet-orthopyroxene gneiss suggest that a precursor aluminous orthopyroxene was present during the ultrahigh-temperature stage.

For the retrograde event, although chemical zoning of major element composition of garnet developed during cooling and reflects high-temperature diffusion, compositional zoning of more slowly diffusing elements, such as Ca, show a complicated pattern caused by partial resorbtion and overgrowth. Garnet rims in all rock types are intergrown with quartz and have relatively high grossular composition. Plagioclase in the garnet-orthopyroxene gneiss and garnet felsic gneiss show reverse zoning. Garnet-amphibole gneiss contains two amphiboles (gedrite and cummingtonite) with different fluorine contents; gedrite occurs as finely crystalline overgrowths surrounding cummingtonite, implying that the retrograde process after peak (ultrahigh-temperature) metamorphism was not simple cooling.

key words: UHT metamorphic rocks, UHT metamorphism, Christmas Point, Napier Complex, East Antarctica

---

* Present address: Nagoya University Center for Chronological Research, Furo-cho, Chikusa-ku, Nagoya 464-8602.

1. Introduction

The Napier complex, a metamorphic terrane that underwent ultrahigh-temperature (UHT) metamorphism, is characterized by mineral assemblages such as sapphirine+quartz, spinel+quartz, orthopyroxene+sillimanite+quartz, and osumilite (*e.g.*, Sheraton *et al.*, 1987; Harley and Hensen, 1990). In recent research, peak metamorphic conditions of the Napier complex have been estimated to have been over 1100°C (Hokada *et al.*, 1999a, b; Harley and Motoyoshi, 2000; Yoshimura *et al.*, 2000). The metamorphic event has been dated at *ca.* 2.4–2.5 Ga (Grew and Manton, 1979; Owada *et al.*, 1994; Tainosho *et al.*, 1994; Shiraishi *et al.*, 1997; Asami *et al.*, 1998; Hokada *et al.*, 2000; Suzuki *et al.*, 2000) and SHRIMP ages when the tonalitic precursor of the orthogneiss intruded into the crust are *ca.* 3.93 Ga (Black *et al.*, 1986) to 3.95 Ga (Williams *et al.*, 1984). This complex is thus important for the study of unusually high temperature metamorphic conditions, and the development and evolution of the Precambrian continental crust. Sheraton *et al.* (1987) and Harley and Hensen (1990) summarized the regional metamorphism of the Napier complex, showed that the most high-grade area is around Amundsen Bay, documented the occurrence of osumilite and the mineral parageneses of sapphirine+quartz and orthopyroxene+sillimanite, and demonstrated the history of Proterozoic reworking and overprinting in the southern part of the complex. The metamorphic history and stages of mineral formation of the Napier complex were proposed by Sheraton *et al.* (1987), Harley and Hensen (1990) and Grew *et al.* (2000), and the southern part of the complex (around Casey Bay) was interpreted to have been reworked under the influence of the adjacent Rayner complex (metamorphic age is *ca.* 1.1 Ga; Black *et al.*, 1983).

Investigation of the geology of the Napier Complex in Enderby Land was carried out by JARE (Japanese Antarctic Research Expedition) under the SEAL (Structure and Evolution of east Antarctic Lithosphere) project, which started in 1996. The project included a field survey of Christmas Point, an area not previously explored by JARE, in 1998–1999 (JARE-40). Sheraton *et al.* (1987) and Harley and Hensen (1990) suggested the possibility of polymetamorphism in the Christmas Point region in the younger (*ca.* 1.1 Ga from Black *et al.*, 1983, 1984) ductile shear zones, which are apparently related to the Rayner metamorphism and structural geologic evidence. Previous work in this region includes a short report on field relations (Black *et al.*, 1983) and investigations of pegmatite and Be-minerals (*e.g.*, Grew, 1981, 1998; Grew *et al.*, 2000), but detailed petrography has not been undertaken. This paper describes the high-grade metamorphic rocks from Christmas Point, and interprets their implications for peak UHT) metamorphism and the retrograde process.

2. Petrography

Christmas Point is located in the southern part of the Napier Complex, Enderby Land, East Antarctica (Fig. 1). This area is the southern part of Field Island (or Ayatollash Island in Black *et al.*, 1983). According to the geological map of Black *et al.* (1983), this area consists predominantly of pinkish garnet-quartz mesoperthitic gneiss. In the field, the study area is dominated by well-layered gneisses, of which garnet-
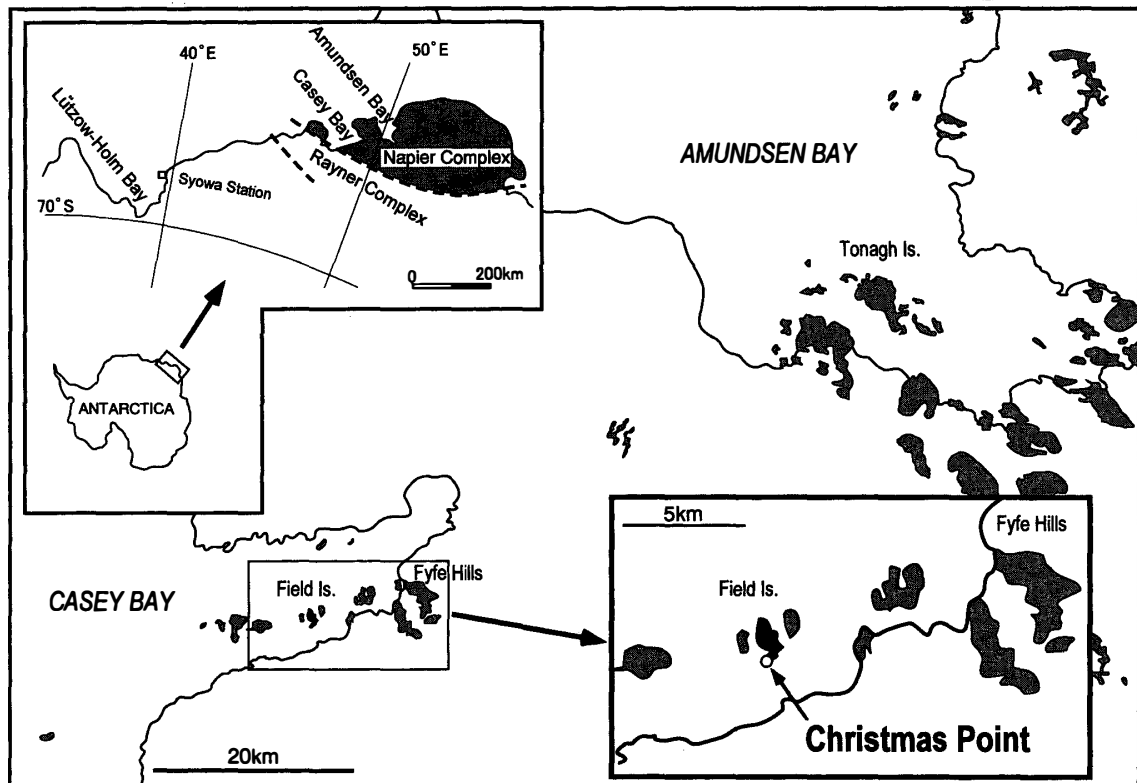
Fig. 1. Location map of Christmas Point in Enderby Land, East Antarctica.

orthopyroxene gneiss and garnet felsic gneiss are the most abundant types. Orthopyroxene-bearing quartz-rich granulite is present as layers within the garnet felsic gneiss. Garnet-amphibole gneiss is present as layers in both the garnet-orthopyroxene gneiss and the garnet felsic gneiss in the southern part of the area (near the grey biotite-muscovite-quartz gneiss of Black *et al.*, 1983). Pegmatites, intruded discontinuously for the layering trend of the host metamorphic rocks, were studied by Grew (1981) and Grew *et al.* (2000).

2.1. Garnet-orthopyroxene gneiss

The layers rich in garnet and/or orthopyroxene are intercalated with felsic layers (Fig. 2a and b). This rock type commonly exhibits gneissose layering (Fig. 2a), although this structure is locally poorly defined (Fig. 2b). This gneiss is rich in coarse crystalline garnet, orthopyroxene, plagioclase and quartz, and contains a small amount of alkali feldspar (mesoperthite). Garnet exsolution lamellae are characteristically found within the coarse crystalline orthopyroxene, and the periphery of primary orthopyroxene crystals is continuously surrounded by finely crystalline garnet (Fig. 3a). Garnet rims are locally intergrown with quartz. The main mineral assemblages are as follows.

garnet+orthopyroxene+plagioclase+mesoperthite+quartz,
garnet+orthopyroxene+plagioclase+quartz.

2.2. Garnet felsic gneiss

The garnet felsic gneiss has gneissic layering and contains coarsely crystalline
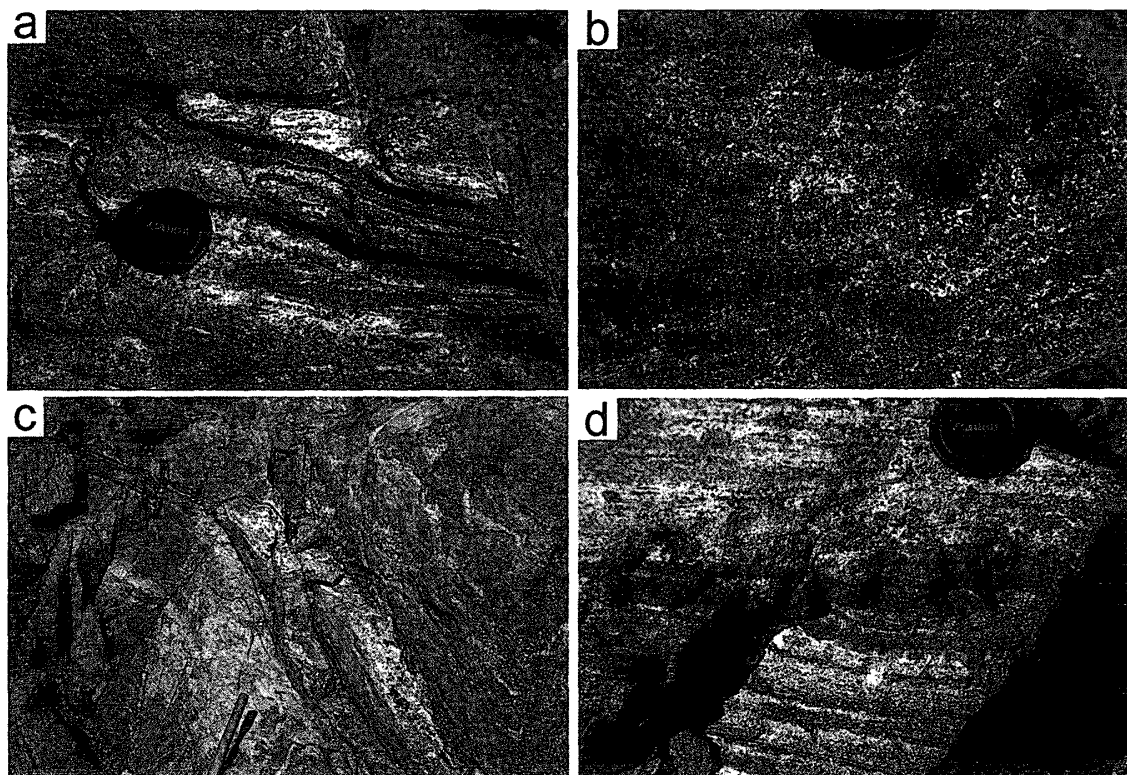
Fig. 2. Modes of occurrence of high-grade metamorphic rocks from Christmas Point. (a) and
(b) Garnet-orthopyroxene gneiss. (c) Garnet felsic gneiss. (d) Garnet-amphibole
gneiss.

leucocratic veins (similar to migmatite leucosomes) that are concordant to, or partly
discordant to, the trend of gneissosity in the host rock (Fig. 2c). The gneiss consists of
garnet, plagioclase, quartz and alkali feldspar (mesoperthite), with a small amount of
orthopyroxene. Garnets are predominantly fine-grained (less than 1 mm diameter), rarely
coarsely crystalline (about 1 cm), and commonly exhibit some intergrowth with quartz in
their rims (Fig. 3b). The main mineral assemblages are as follows.

garnet+orthopyroxene+plagioclase+mesoperthite+ quartz,
garnet+orthopyroxene+plagioclase+quartz,
garnet+plagioclase+mesoperthite+ quartz.

2.3. Orthopyroxene-bearing quartz-rich granulite

Orthopyroxene-bearing quartz-rich granulite consists predominantly of quartz, with
minor amounts of orthopyroxene and sillimanite. Layering is indistinct to massive. This
rock type has limited distribution, and is present most commonly within bodies of garnet
felsic gneiss. Minerals consistently present are medium-crystalline orthopyroxene (0.5–1
mm in size), sillimanite and quartz. Sillimanite is present in two crystal sizes: one is
coarsely crystalline (about 0.5 mm) and exhibits a granoblastic texture with
orthopyroxene, whereas the other is very finely crystalline (about 50 μm or smaller) and
is present around the periphery of orthopyroxene crystals (Fig. 3c, d). Sapphirine is
present as inclusions in the coarsely crystalline sillimanite (Fig. 3d). Biotite forms
around orthopyroxene and sillimanite. The main mineral assemblages are as follows.
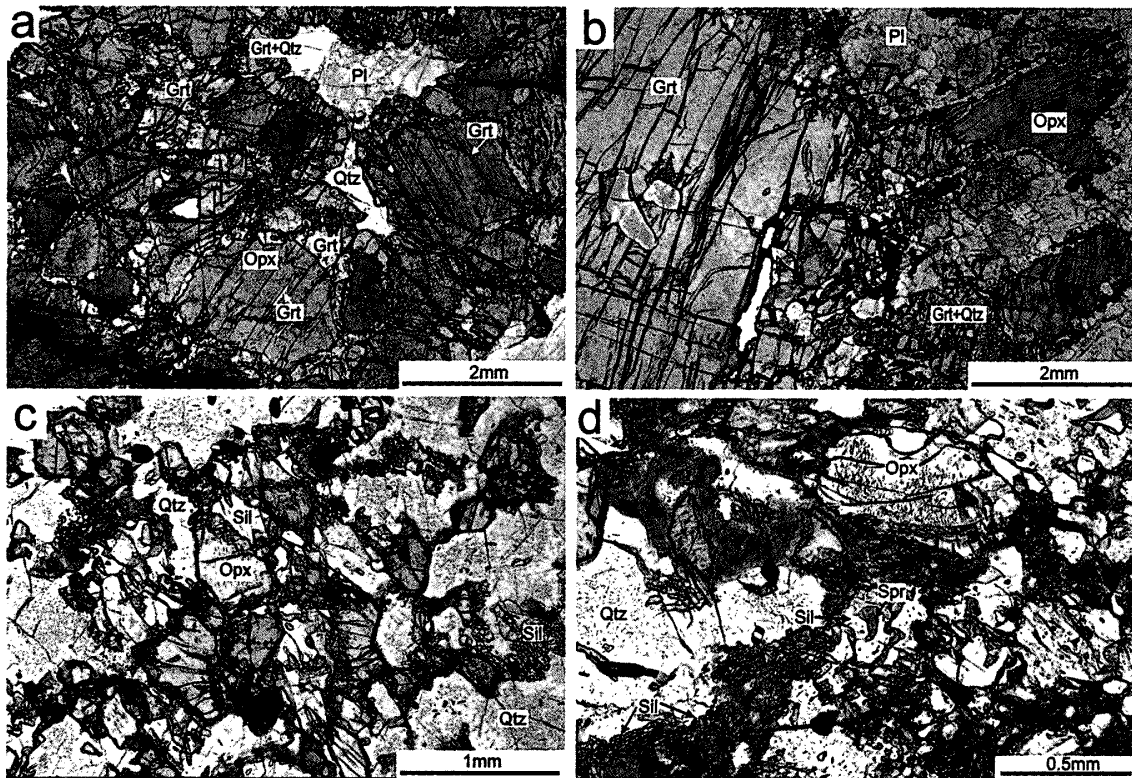
Fig. 3. Photomicrographs of garnet-orthopyroxene gneiss, garnet felsic gneiss and orthopyroxene-bearing quartz-rich granulite from Christmas Point. (a) Garnet-orthopyroxene gneiss. Garnet exsolution lamellae are present in orthopyroxene, and the peripheries of primary orthopyroxene crystals are surrounded by fine-grain garnet. (b) Garnet felsic gneiss. Note symplectitic intergrowth of garnet and quartz. (c) and (d) Orthopyroxene-bearing quartz-rich granulite. Sillimanite has two distinct crystal sizes. Sapphirine inclusions are present in the sillimanite. Grt: garnet, Opx: orthopyroxene, Pl: plagioclase, Qtz: quartz, Sil: sillimanite, Spr: sapphirine.

orthopyroxene+sillimanite+plagioclase+quartz,

orthopyroxene+sillimanite+quartz,

orthopyroxene+sillimanite+biotite+quartz.

2.4. Garnet-amphibole gneiss

Garnet-amphibole gneiss has well-developed gneissose structure, and is rich in garnet, amphibole and quartzo-feldspathic layers (Fig. 2d). This rock type consists predominantly of garnet, amphibole (gedrite and cummingtonite), biotite, plagioclase and quartz, with minor amounts of K-feldspar. Cummingtonite commonly occurs as aggregates of acicular crystals in the quartzo-feldspathic layers (Fig. 4). Gedrite is present as euhedral crystals around the margins of garnet and as finely crystalline overgrowths surrounding cummingtonite (Fig. 4). Euhedral gedrite coexists with cummingtonite in the same thin section. Biotite is present around the garnets and amphiboles. Garnets are predominantly fine-grained (less than 1.5 mm diameter), and commonly show some intergrowth with quartz (Fig. 4a and c). The main mineral assemblages are as follows.

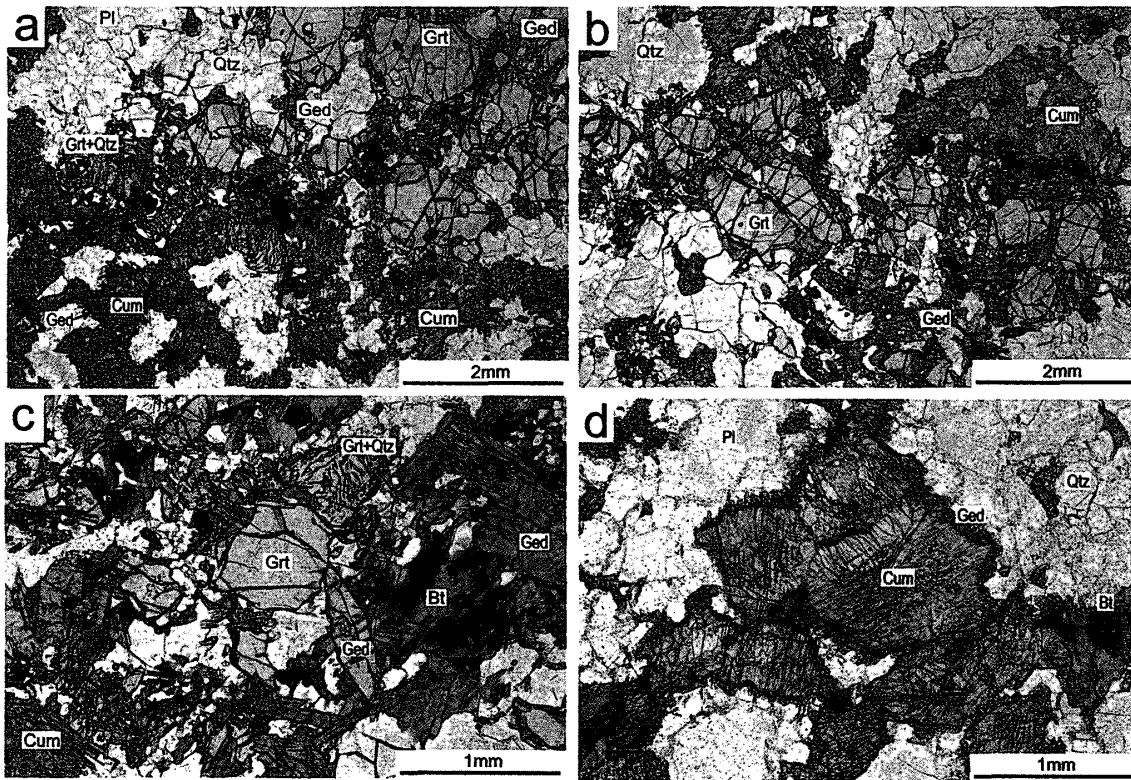garnet+cummingtonite+gedrite+plagioclase+K-feldspar+quartz,

Fig. 4. Photomicrograph of garnet-amphibole gneiss. (a) and (b) Cummingtonite commonly occurs as an aggregate of acicular crystals. (c) Euhedral gedrite coexists with cummingtonite. (d) Gedrite occurs as fine crystals, and as overgrowths on cummingtonite. Cum: cummingtonite, Ged: gedrite, Bt: biotite.

garnet+cummingtonite+gedrite+biotite+plagioclase+quartz,
garnet+cummingtonite+gedrite+biotite+plagioclase.

3. Mineral chemistry

3.1. Analytical techniques

Mineral chemical compositions were obtained using a wave-length dispersive electron probe microanalyzer (JEOL JXA-8600M) at Kochi University. For quantitative analyses, an acceleration voltage of 15 kV, probe current of 1.5×10^{-8} A, and beam diameter of 1 or 5 μm were used. Oxide ZAF correction was applied to the data. For compositional mapping, an acceleration voltage of 15 kV, probe current of 7.5×10^{-7} A, dwell time of 50 ms and beam diameter of 5 μm were used. The compositions of the analyzed minerals are shown in Table 1.

3.2. Mineral compositions
3.2.1. Garnet

Garnet chemical compositions are shown in Prp-Alm-Sps and Prp-Alm-Grs diagrams (Fig. 5). Garnet core compositions from garnet-orthopyroxene gneiss, garnet felsic gneiss and garnet-amphibole gneiss are $Prp_{45-53}Alm_{43-48}Sps_1Grs_{5-9}$, $Prp_{45-50}Alm_{43-46}Sps_1Grs_{5-9}$ and $Prp_{35-45}Alm_{48-60}Sps_1Grs_{5-7}$, respectively. In all of the rock types, Mg contents are highest

Table. 1. *Representative electron microprobe analysis of minerals in garnet-orthopyroxene gneiss, garnet felsic gneiss, orthopyroxene-bearing quartz-rich granulite and garnet amphibole gneiss from Christmas Point.*

mineral	Garnet (O=12)														
rock type	Grt-Opx gneiss					Grt-felsic gneiss					Grt-Amp gneiss				
sample	9901220801					9901220707					9901220206		9901220211		
SiO_2	40.58	40.24	40.38	40.25	40.25	39.74	40.24	40.17	40.11	39.64	39.84	39.27	39.79	39.32	39.06
TiO_2	0.00	0.03	0.01	0.00	0.00	0.02	0.01	0.01	0.01	0.01	0.00	0.00	0.00	0.03	0.00
Al_2O_3	22.85	22.96	22.62	22.69	22.66	22.29	22.81	22.87	22.57	22.52	22.40	22.31	22.43	22.18	22.15
Cr_2O_3	0.02	0.07	0.03	0.01	0.00	0.03	0.03	0.04	0.04	0.01	0.03	0.04	0.01	0.05	0.00
FeO*	21.73	21.19	20.97	20.73	21.59	21.81	21.72	20.43	21.87	20.88	24.13	26.95	23.39	28.77	26.54
MnO	0.28	0.23	0.27	0.34	0.28	0.30	0.32	0.35	0.35	0.28	0.17	0.26	0.18	0.36	0.24
NiO	0.00	0.00	0.00	0.00	0.00	0.00	0.00	0.00	0.00	0.00	0.00	0.00	0.00	0.00	0.03
MgO	13.43	14.34	13.93	14.10	12.38	12.57	13.47	13.64	13.43	12.86	11.96	9.33	12.65	8.33	9.29
CaO	2.55	1.87	2.23	2.12	3.35	3.31	2.14	2.30	2.17	2.88	2.01	2.06	2.10	2.23	2.25
Na_2O	0.01	0.00	0.00	0.02	0.01	0.00	0.01	0.01	0.00	0.00	0.02	0.02	0.01	0.01	0.00
K_2O	0.00	0.00	0.00	0.00	0.00	0.00	0.00	0.00	0.00	0.00	0.00	0.00	0.00	0.00	0.00
P_2O_5	0.02	0.05	0.01	0.07	0.03	0.07	0.04	0.01	0.05	0.08	0.10	0.12	0.02	0.03	0.05
Total	101.47	100.96	100.45	100.33	100.56	100.12	100.79	99.83	100.60	99.16	100.66	100.36	100.59	101.32	99.61
Si	2.991	2.970	2.996	2.987	3.001	2.983	2.985	2.993	2.986	2.987	2.991	2.998	2.982	3.002	3.004
Ti	0.000	0.001	0.000	0.000	0.000	0.001	0.000	0.001	0.001	0.001	0.000	0.000	0.000	0.002	0.000
Al	1.985	1.997	1.978	1.984	1.991	1.972	1.994	2.008	1.980	2.000	1.982	2.008	1.981	1.995	2.007
Cr	0.001	0.004	0.002	0.001	0.000	0.001	0.002	0.002	0.003	0.001	0.002	0.002	0.001	0.003	0.000
Fe^{2+}	1.339	1.308	1.301	1.287	1.346	1.369	1.348	1.273	1.361	1.316	1.515	1.720	1.466	1.837	1.707
Mn	0.018	0.014	0.017	0.021	0.018	0.019	0.020	0.022	0.022	0.018	0.011	0.017	0.011	0.023	0.016
Ni	0.000	0.000	0.000	0.000	0.000	0.000	0.000	0.000	0.000	0.000	0.000	0.000	0.000	0.000	0.002
Mg	1.475	1.578	1.541	1.560	1.375	1.406	1.490	1.515	1.490	1.445	1.338	1.062	1.413	0.947	1.065
Ca	0.202	0.147	0.177	0.169	0.268	0.266	0.170	0.184	0.173	0.233	0.162	0.169	0.168	0.183	0.185
Na	0.001	0.000	0.000	0.003	0.001	0.000	0.001	0.001	0.000	0.000	0.003	0.003	0.001	0.002	0.000
K	0.000	0.000	0.000	0.000	0.000	0.000	0.000	0.000	0.000	0.000	0.000	0.000	0.000	0.000	0.000
P	0.001	0.003	0.001	0.004	0.002	0.004	0.002	0.001	0.003	0.005	0.006	0.007	0.001	0.002	0.003
Total	8.014	8.023	8.013	8.015	8.001	8.023	8.013	8.000	8.018	8.004	8.009	7.987	8.026	7.995	7.988
X_{Mg}	0.52	0.55	0.54	0.55	0.51	0.51	0.53	0.54	0.52	0.52	0.47	0.38	0.49	0.34	0.38
Prp	48.63	51.78	50.76	51.37	45.73	45.95	49.21	50.59	48.91	47.98	44.22	35.79	46.20	31.69	35.84
Alm	44.14	42.91	42.85	42.37	44.77	44.73	44.51	42.52	44.68	43.71	50.07	57.96	47.92	61.43	57.40
Sps	0.58	0.47	0.56	0.70	0.59	0.63	0.66	0.74	0.73	0.58	0.37	0.57	0.38	0.77	0.53
Grs	6.64	4.84	5.83	5.55	8.91	8.69	5.62	6.14	5.68	7.72	5.34	5.69	5.50	6.11	6.24

*=Total Fe as FeO

Table 1. Continued.

mineral	Orthopyroxene (O=6)														
rock type	Grt-Opx gneiss					Grt-felsic gneiss					Opx granulite				
sample	9901220801					9901220701		9901220707			9901220402		9901220404		
SiO$_2$	51.98	51.19	51.36	51.01	51.90	51.76	51.70	51.67	51.48	50.88	52.66	52.81	52.39	52.12	51.80
TiO$_2$	0.04	0.02	0.04	0.08	0.01	0.05	0.05	0.07	0.05	0.05	0.07	0.06	0.04	0.08	0.05
Al$_2$O$_3$	4.46	5.74	6.08	5.91	4.85	5.03	5.11	5.29	5.04	5.39	7.11	6.22	7.21	7.56	7.93
Cr$_2$O$_3$	0.02	0.03	0.06	0.02	0.00	0.04	0.01	0.06	0.00	0.00	0.00	0.02	0.05	0.02	0.00
FeO*	16.54	16.95	16.59	17.01	16.19	17.75	18.43	18.29	18.94	19.41	11.49	10.55	10.48	10.69	11.15
MnO	0.12	0.03	0.07	0.08	0.00	0.11	0.09	0.11	0.13	0.11	0.09	0.08	0.00	0.11	0.04
NiO	0.03	0.00	0.09	0.04	0.00	0.00	0.00	0.01	0.06	0.03	0.00	0.04	0.04	0.01	0.05
MgO	26.21	25.15	24.91	25.17	26.38	25.30	24.99	24.83	24.20	24.02	29.44	29.74	29.80	29.61	29.55
CaO	0.15	0.15	0.15	0.14	0.10	0.14	0.13	0.14	0.14	0.12	0.08	0.07	0.05	0.03	0.04
Na$_2$O	0.00	0.02	0.01	0.00	0.01	0.00	0.01	0.00	0.00	0.00	0.00	0.00	0.00	0.00	0.00
K$_2$O	0.00	0.00	0.00	0.00	0.00	0.00	0.00	0.00	0.00	0.00	0.00	0.00	0.00	0.00	0.00
P$_2$O$_5$	0.03	0.01	0.01	0.00	0.02	0.04	0.00	0.01	0.00	0.00	0.01	0.01	0.01	0.00	0.01
Total	99.57	99.28	99.37	99.45	99.46	100.22	100.52	100.46	100.05	100.01	100.96	99.60	100.06	100.23	100.63
Si	1.888	1.867	1.868	1.859	1.882	1.877	1.875	1.874	1.881	1.865	1.841	1.863	1.839	1.829	1.815
Ti	0.001	0.001	0.001	0.002	0.000	0.001	0.001	0.002	0.001	0.001	0.002	0.001	0.001	0.002	0.001
Al	0.191	0.247	0.260	0.254	0.207	0.215	0.218	0.226	0.217	0.233	0.293	0.259	0.298	0.313	0.327
Cr	0.001	0.001	0.002	0.001	0.000	0.001	0.000	0.002	0.000	0.000	0.000	0.001	0.001	0.001	0.000
Fe^{2+}	0.502	0.517	0.505	0.518	0.491	0.539	0.559	0.555	0.579	0.595	0.336	0.311	0.308	0.314	0.327
Mn	0.004	0.001	0.002	0.002	0.000	0.003	0.003	0.003	0.004	0.003	0.003	0.002	0.000	0.003	0.001
Ni	0.001	0.000	0.003	0.001	0.000	0.000	0.000	0.000	0.002	0.001	0.000	0.001	0.001	0.000	0.001
Mg	1.420	1.368	1.351	1.368	1.426	1.368	1.351	1.343	1.319	1.313	1.534	1.564	1.560	1.549	1.543
Ca	0.006	0.006	0.006	0.006	0.004	0.005	0.005	0.005	0.006	0.005	0.003	0.003	0.002	0.001	0.002
Na	0.000	0.001	0.001	0.000	0.001	0.000	0.000	0.000	0.000	0.000	0.000	0.000	0.000	0.000	0.000
K	0.000	0.000	0.000	0.000	0.000	0.000	0.000	0.000	0.000	0.000	0.000	0.000	0.000	0.000	0.000
P	0.001	0.000	0.000	0.000	0.001	0.001	0.000	0.000	0.000	0.000	0.000	0.000	0.000	0.000	0.000
Total	4.014	4.008	3.999	4.011	4.013	4.011	4.014	4.010	4.009	4.017	4.011	4.006	4.010	4.012	4.019
X$_{Mg}$	0.74	0.73	0.73	0.73	0.74	0.72	0.71	0.71	0.69	0.69	0.82	0.83	0.84	0.83	0.83
En	73.64	72.35	72.57	72.30	74.24	71.55	70.55	70.57	69.29	68.63	81.91	83.29	83.43	83.11	82.45
Fs	26.07	27.34	27.11	27.41	25.56	28.17	29.19	29.15	30.42	31.11	17.93	16.57	16.46	16.83	17.46
Wo	0.29	0.30	0.32	0.29	0.20	0.28	0.26	0.28	0.29	0.25	0.16	0.14	0.11	0.05	0.09

*=Total Fe as FeO

Table 1. Continued.

mineral	Plagioclase (O=8)														
rock type	Grt-Opx gneiss				Grt-felsic gneiss						Grt-Amp gneiss				
sample	9901220801				9901220701		9901220707				9901220206			9901220211	
SiO$_2$	54.22	52.06	54.50	49.02	47.75	53.68	47.21	53.84	49.05	54.24	56.38	56.22	55.81	56.53	56.18
TiO$_2$	0.00	0.03	0.00	0.05	0.02	0.00	0.00	0.01	0.00	0.00	0.00	0.02	0.01	0.00	0.01
Al$_2$O$_3$	28.74	30.54	28.72	31.48	32.84	29.16	33.13	28.78	32.44	28.47	27.38	27.72	27.64	27.26	27.44
Cr$_2$O$_3$	0.00	0.01	0.04	0.02	0.00	0.00	0.00	0.00	0.00	0.00	0.05	0.00	0.00	0.00	0.05
FeO*	0.03	0.25	0.06	0.22	0.07	0.03	0.24	0.04	0.10	0.06	0.03	0.16	0.29	0.02	0.02
MnO	0.02	0.00	0.01	0.00	0.01	0.02	0.00	0.00	0.02	0.00	0.00	0.06	0.00	0.02	0.00
NiO	0.04	0.00	0.00	0.02	0.00	0.00	0.02	0.00	0.00	0.00	0.01	0.00	0.00	0.00	0.01
MgO	0.00	0.00	0.02	0.01	0.03	0.01	0.00	0.00	0.00	0.00	0.00	0.02	0.00	0.00	0.00
CaO	11.47	13.69	11.63	15.82	16.29	11.68	16.85	11.76	15.51	11.28	10.10	10.18	10.25	9.60	9.73
Na$_2$O	5.10	3.95	4.86	2.75	2.25	4.87	1.97	4.91	2.57	5.07	6.11	6.02	5.76	6.37	6.13
K$_2$O	0.11	0.11	0.14	0.01	0.01	0.14	0.03	0.24	0.07	0.23	0.07	0.03	0.06	0.05	0.07
P$_2$O$_5$	0.03	0.02	0.02	0.28	0.00	0.02	0.02	0.04	0.00	0.02	0.07	0.02	0.05	0.02	0.01
Total	99.76	100.67	99.98	99.67	99.26	99.61	99.46	99.60	99.76	99.36	100.20	100.44	99.86	99.87	99.65
Si	2.455	2.353	2.461	2.251	2.204	2.435	2.180	2.445	2.246	2.465	2.531	2.520	2.516	2.543	2.534
Ti	0.000	0.001	0.000	0.002	0.001	0.000	0.000	0.000	0.000	0.000	0.000	0.001	0.000	0.000	0.000
Al	1.533	1.627	1.528	1.704	1.786	1.559	1.803	1.540	1.751	1.525	1.449	1.464	1.469	1.445	1.459
Cr	0.000	0.000	0.001	0.001	0.000	0.000	0.000	0.000	0.000	0.000	0.002	0.000	0.000	0.000	0.002
Fe^{2+}	0.001	0.010	0.002	0.008	0.003	0.001	0.009	0.002	0.004	0.002	0.001	0.006	0.011	0.001	0.001
Mn	0.001	0.000	0.000	0.000	0.000	0.001	0.000	0.000	0.001	0.000	0.000	0.002	0.000	0.001	0.000
Ni	0.001	0.000	0.000	0.001	0.000	0.000	0.001	0.000	0.000	0.000	0.000	0.000	0.000	0.000	0.000
Mg	0.000	0.000	0.001	0.000	0.002	0.000	0.000	0.000	0.000	0.000	0.000	0.001	0.000	0.000	0.000
Ca	0.556	0.663	0.562	0.778	0.806	0.568	0.834	0.572	0.761	0.549	0.486	0.489	0.495	0.463	0.470
Na	0.448	0.346	0.426	0.244	0.201	0.429	0.176	0.432	0.228	0.447	0.532	0.524	0.504	0.556	0.536
K	0.006	0.006	0.008	0.001	0.001	0.008	0.002	0.014	0.004	0.013	0.004	0.002	0.003	0.003	0.004
P	0.001	0.001	0.001	0.011	0.000	0.001	0.001	0.001	0.000	0.001	0.003	0.001	0.002	0.001	0.000
Total	5.004	5.007	4.990	5.001	5.003	5.002	5.006	5.006	4.995	5.002	5.008	5.009	5.000	5.012	5.006
Ab	44.32	34.08	42.73	23.89	19.99	42.68	17.44	42.44	22.94	44.29	52.04	51.63	50.26	54.42	53.06
An	55.06	65.30	56.47	76.03	79.95	56.52	82.37	56.21	76.63	54.40	47.55	48.21	49.40	45.30	46.52
Or	0.62	0.62	0.80	0.08	0.06	0.80	0.19	1.35	0.42	1.31	0.41	0.16	0.34	0.28	0.42

*=Total Fe as FeO

Table 1. Continued.

| mineral	Amphibole (O=23)												Biotite (O=22)					
rock type	Grt-Amp gneiss												Grt-Amp gneiss					
sample	9901220206						9901220211						9901220206			9901220211		
	comingtonite			gedrite			comingtonite			gedrite								
SiO$_2$	52.09	51.86	53.19	45.69	45.32	47.38	51.16	52.46	51.98	46.05	45.05	46.06	39.24	39.02	39.62	38.91	38.78	39.75
TiO$_2$	0.09	0.12	0.13	0.23	0.21	0.18	0.17	0.10	0.18	0.16	0.20	0.20	2.59	2.68	2.43	2.50	2.75	2.71
Al$_2$O$_3$	5.57	6.20	5.35	14.89	15.21	13.71	6.43	4.88	6.65	13.89	14.64	13.42	17.47	17.06	16.98	17.23	17.06	17.30
Cr$_2$O$_3$	0.14	0.11	0.11	0.13	0.08	0.06	0.04	0.00	0.05	0.07	0.02	0.00	0.16	0.19	0.21	0.18	0.08	0.04
FeO*	16.99	17.56	16.55	17.31	16.68	16.56	17.97	17.31	17.25	17.24	17.14	17.57	10.63	11.23	10.06	10.73	12.36	11.61
MnO	0.08	0.01	0.00	0.10	0.00	0.03	0.09	0.01	0.10	0.08	0.04	0.07	0.02	0.00	0.03	0.03	0.00	0.01
NiO	0.00	0.00	0.01	0.05	0.00	0.00	0.00	0.00	0.00	0.04	0.01	0.00	0.00	0.07	0.00	0.01	0.00	0.04
MgO	21.22	20.91	21.30	18.02	17.76	18.90	20.53	21.45	20.99	17.82	17.69	18.19	17.56	17.52	17.84	16.91	16.51	17.19
CaO	0.35	0.31	0.34	0.42	0.67	0.44	0.29	0.26	0.35	0.43	0.53	0.56	0.12	0.18	0.03	0.02	0.01	0.06
Na$_2$O	0.38	0.42	0.34	1.10	0.99	1.20	0.55	0.31	0.54	1.20	1.26	1.11	0.17	0.18	0.14	0.24	0.22	0.15
K$_2$O	0.00	0.00	0.00	0.00	0.00	0.00	0.00	0.00	0.00	0.00	0.00	0.00	7.63	7.22	7.37	8.33	7.95	7.45
P$_2$O$_5$	0.17	0.01	0.04	0.00	0.00	0.01	0.03	0.03	0.00	0.02	0.02	0.00	0.02	0.01	0.04	0.00	0.02	0.00
F	0.00	0.00	0.00	0.15	0.20	0.12	0.00	0.00	0.00	0.13	0.27	0.30	0.49	0.72	0.22	0.46	0.21	0.34
O=	0.00	0.00	0.00	-0.06	-0.08	-0.05	0.00	0.00	0.00	-0.05	-0.11	-0.12	-0.21	-0.30	-0.09	-0.19	-0.09	-0.14
Total	97.08	97.52	97.36	98.03	97.04	98.53	97.26	96.81	98.09	97.09	96.77	97.35	95.89	95.78	94.88	95.35	95.86	96.51
Si	7.426	7.380	7.526	6.520	6.513	6.685	7.327	7.503	7.346	6.631	6.521	6.634	5.616	5.609	5.691	5.631	5.605	5.659
Ti	0.010	0.013	0.014	0.025	0.022	0.019	0.018	0.011	0.019	0.018	0.022	0.022	0.279	0.290	0.263	0.272	0.299	0.290
Al	0.935	1.041	0.893	2.503	2.576	2.279	1.084	0.822	1.107	2.357	2.497	2.277	2.946	2.891	2.875	2.938	2.905	2.902
Cr	0.016	0.012	0.012	0.015	0.009	0.007	0.005	0.000	0.005	0.008	0.003	0.000	0.018	0.021	0.024	0.020	0.009	0.005
Fe^{2+}	2.026	2.090	1.958	2.066	2.005	1.954	2.152	2.070	2.039	2.076	2.075	2.116	1.272	1.350	1.208	1.299	1.493	1.382
Mn	0.009	0.001	0.000	0.012	0.000	0.004	0.011	0.001	0.012	0.010	0.005	0.009	0.003	0.000	0.004	0.003	0.000	0.002
Ni	0.000	0.000	0.001	0.005	0.000	0.000	0.000	0.000	0.000	0.005	0.002	0.000	0.000	0.008	0.000	0.001	0.000	0.005
Mg	4.510	4.435	4.492	3.833	3.805	3.974	4.384	4.574	4.422	3.825	3.817	3.905	3.745	3.756	3.820	3.648	3.556	3.648
Ca	0.054	0.048	0.051	0.064	0.104	0.066	0.044	0.039	0.053	0.066	0.083	0.087	0.018	0.028	0.004	0.003	0.001	0.009
Na	0.104	0.116	0.094	0.305	0.276	0.327	0.152	0.087	0.147	0.336	0.353	0.309	0.047	0.051	0.038	0.066	0.062	0.043
K	0.000	0.000	0.000	0.000	0.000	0.000	0.000	0.000	0.000	0.000	0.000	0.000	1.393	1.324	1.351	1.538	1.466	1.352
P	0.021	0.001	0.005	0.000	0.000	0.001	0.004	0.004	0.000	0.002	0.002	0.000	0.003	0.001	0.005	0.000	0.002	0.000
Total	15.110	15.137	15.047	15.349	15.310	15.316	15.180	15.112	15.152	15.333	15.380	15.360	15.340	15.330	15.284	15.420	15.400	15.295
X$_{Mg}$	0.69	0.68	0.70	0.65	0.65	0.67	0.67	0.69	0.68	0.65	0.65	0.65	0.75	0.74	0.76	0.74	0.70	0.73

*=Total Fe as FeO
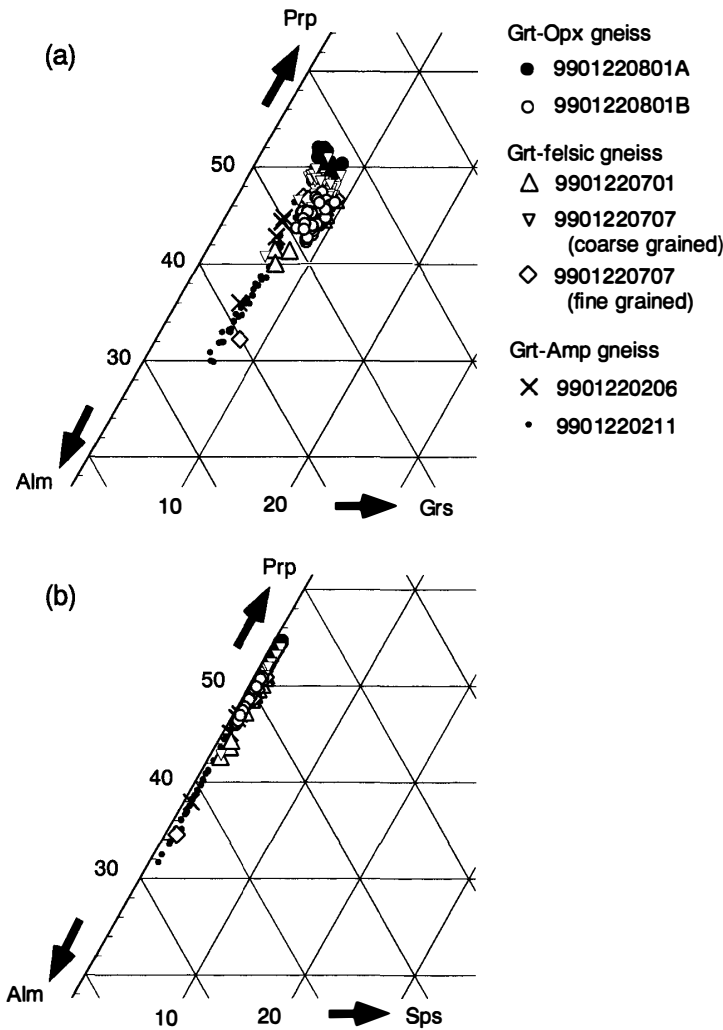
Fig. 5.   *(a) Pyrope (Prp)–almandine (Alm)–grossular (Grs) diagram of garnet composition of rocks from Christmas Point. (b) Pyrope (Prp)–almandine (Alm)–spessartine (Sps) diagram of garnet composition of rocks from Christmas Point.*

in the cores and decrease gradually toward the rims. Chemical zoning of major element composition developed during cooling, and reflects high-temperature diffusion. Grossular content is slightly higher near the rim in the garnet-orthopyroxene gneiss and garnet felsic gneiss. Especially, the Ca content is clearly high for the quartz intergrowth part (Fig. 6). In the garnet-amphibole gneiss, grossular content increases slightly toward the rim. Mn contents are minimal in all rock types. Although the garnets in the garnet felsic gneiss appear to be single crystals both under the microscope and in compositional maps of the relatively quickly diffusing elements (Mg and Fe), compositional zoning of more slowly diffusing elements, such as Ca (Fig. 6), shows complicated pattern caused by partial resorbtion and overgrowth.
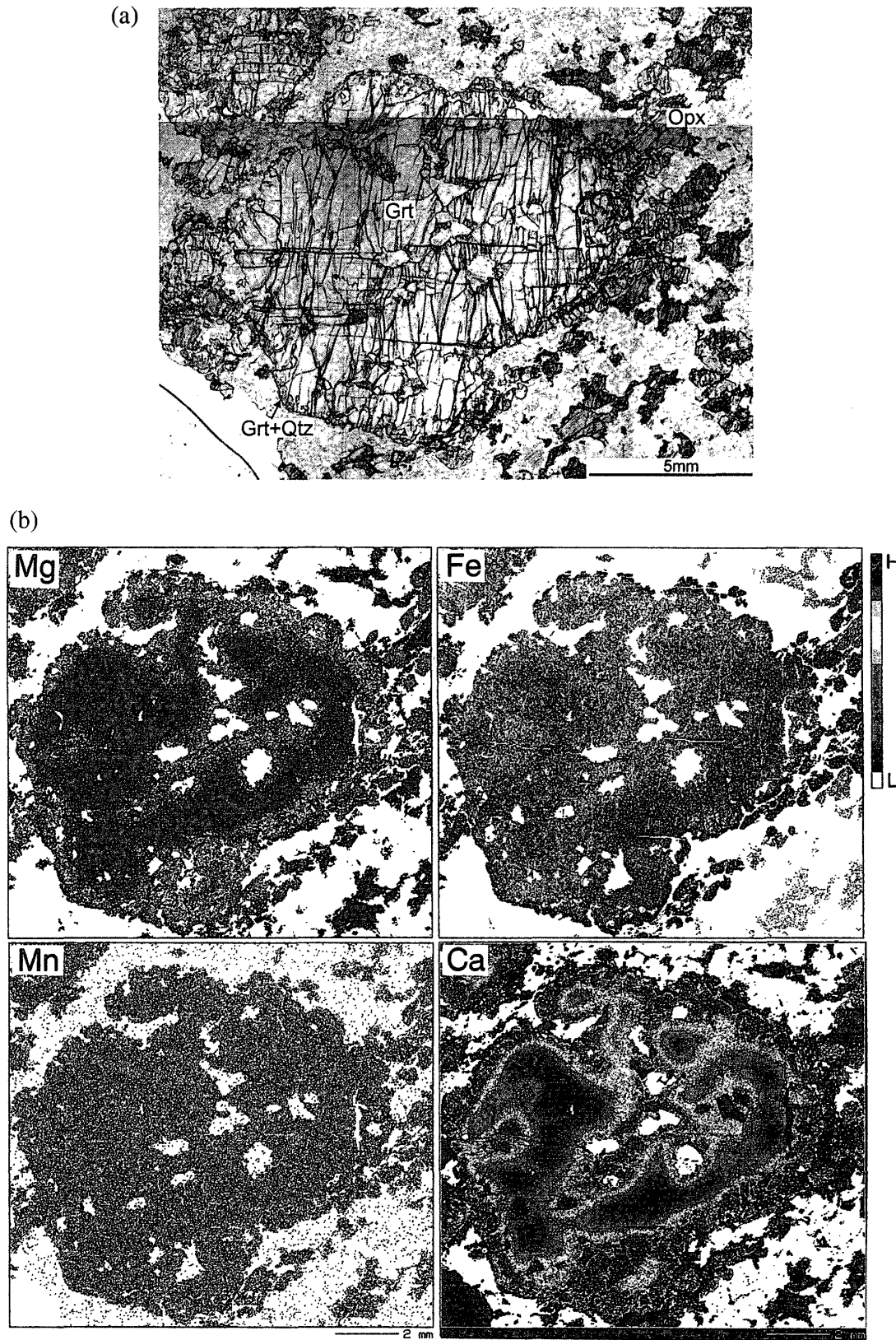
Fig. 6. (a) Photomicrograph of garnet felsic gneiss from Christmas Point (sample
9901220707). (b) compositional color maps of the same garnet crystal as in (a). **H**
represents higher-concentration and **L** is lower-concentration of each element.
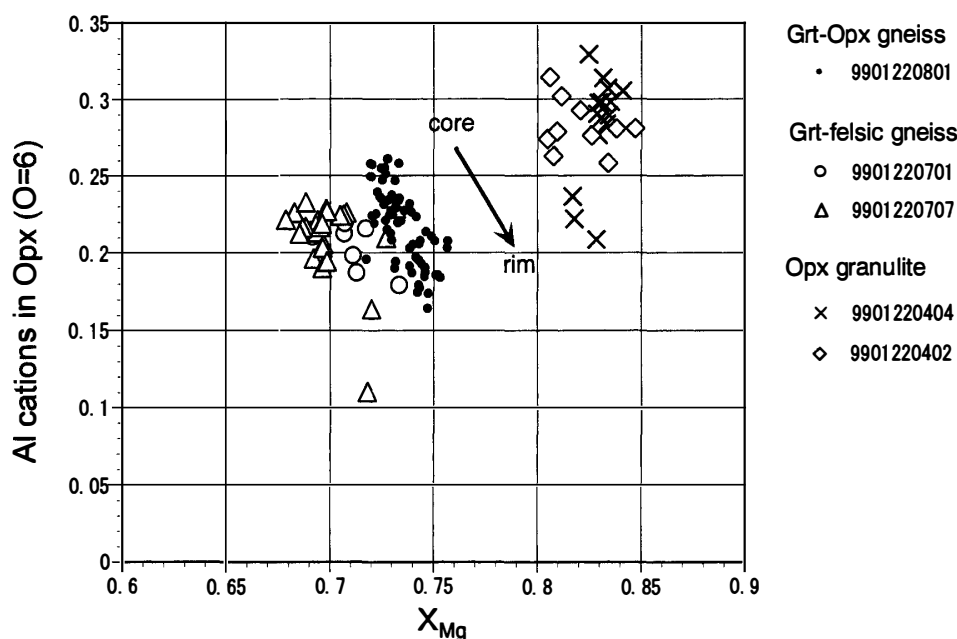
Fig. 7.   Variations in Al content (per 6-oxygen formula unit) and X_{Mg} of orthopyroxene in the rocks from Christmas Point.

3.2.2. Orthopyroxene

The X_{Mg}-Al plot for orthopyroxene is shown in Fig. 7. X_{Mg} of orthopyroxene in the garnet-orthopyroxene gneiss ranges from 0.73 to 0.76, and those in the garnet felsic gneiss range from 0.68 to 0.74. Maximum contents of Al_2O_3 in the orthopyroxene from the garnet-orthopyroxene gneiss and the garnet felsic gneiss are about 6 and 5.3 wt%, respectively. In the orthopyroxene-bearing quartz-rich granulite, the X_{Mg} value ranges from 0.8 to 0.85, and the maximum Al_2O_3 content is about 7.9 wt%, which is the highest value in any of the rock types. Orthopyroxene generally shows compositional zoning, with Al contents highest in the core and decreasing toward the rim. The X_{Mg} value is lowest in the core, and increases toward the rim. In orthopyroxene-bearing quartz-rich granulite, however, a clear change of X_{Mg} is not observed. Orthopyroxene in the garnet-orthopyroxene gneiss includes garnet exsolution lamellae, and compositional maps of such crystals are shown in Fig. 8. The color maps show that Mg increases toward the rim, whereas Al decrease toward the rim, and also decreases slightly near garnet exsolution lamellae.

3.2.3. Plagioclase

The An and Or contents of plagioclase are shown in Fig. 9. The An content of plagioclase from garnet-orthopyroxene gneiss and garnet felsic gneiss is higher than that of plagioclase from garnet-amphibole gneiss. Plagioclase compositions from the garnet-orthopyroxene gneiss are about An54-59 in cores and An54-76 in rims, from the garnet felsic gneiss about An52-58 in cores and An60-84 in rims, and from the garnet-amphibole gneiss about An45-49 in cores and An44-50 in rims. Plagioclase in the garnet-orthopyroxene gneiss and garnet felsic gneiss has a prominent reverse zoning, with Ca content lowest in cores and increasing outward (Fig. 10). Plagioclase that contain antiperthite show this reverse zoning, and are rounded and finely crystalline. In the
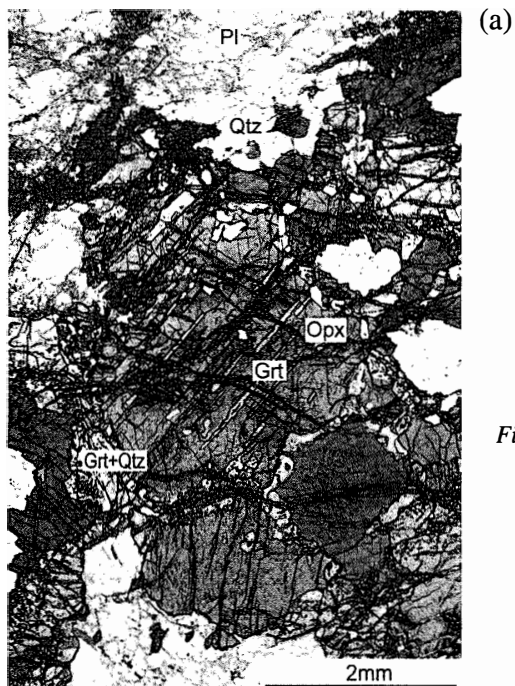
Fig. 8. (a) Photomicrograph of garnet-orthopyroxene gneiss from Christmas Point showing exsolution of garnet in orthopyroxene (sample 9901220801). (b) Color composition maps of the same crystal as in (a). Tow composition map of Al changed the compositional range in order to do comprehensible the kind and the distribution of the minerals around of the orthopyroxene. **H** represents higher-concentration and **L** is lower-concentration of each element.
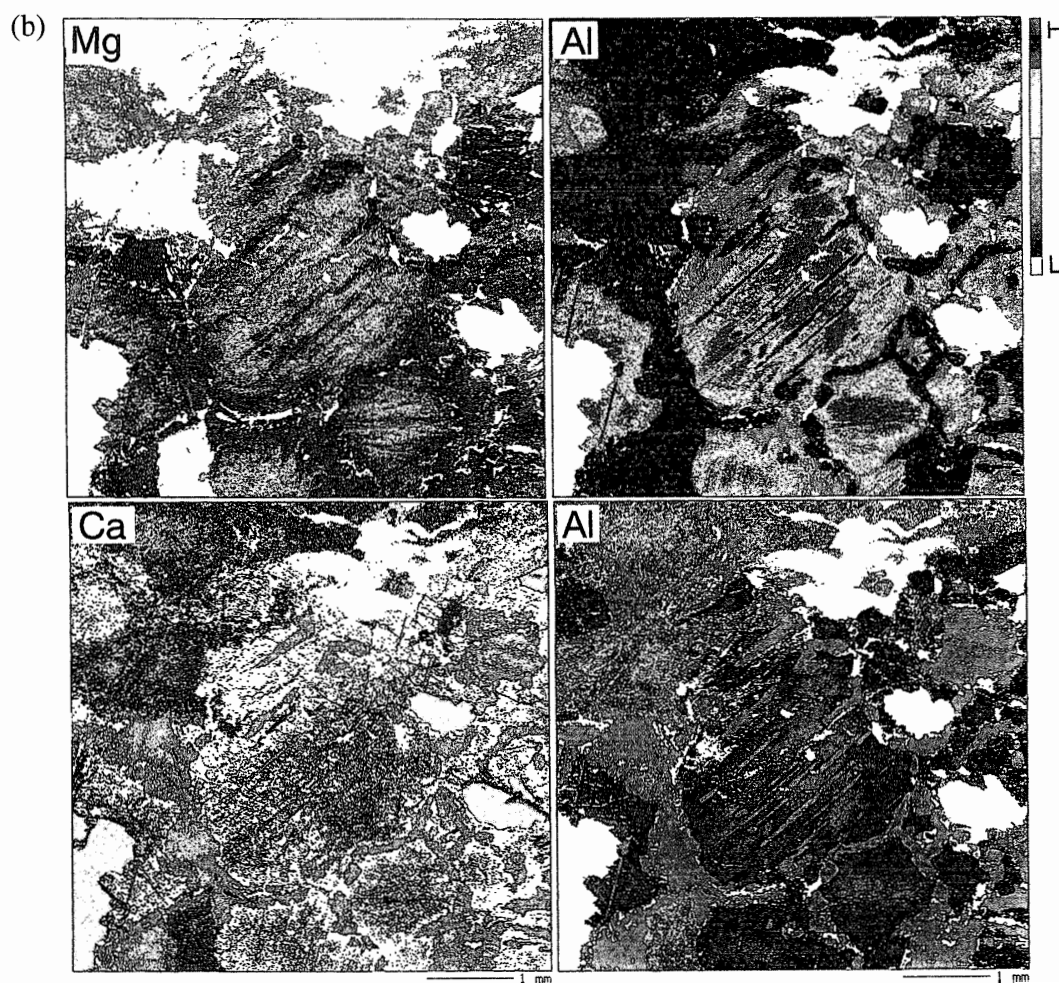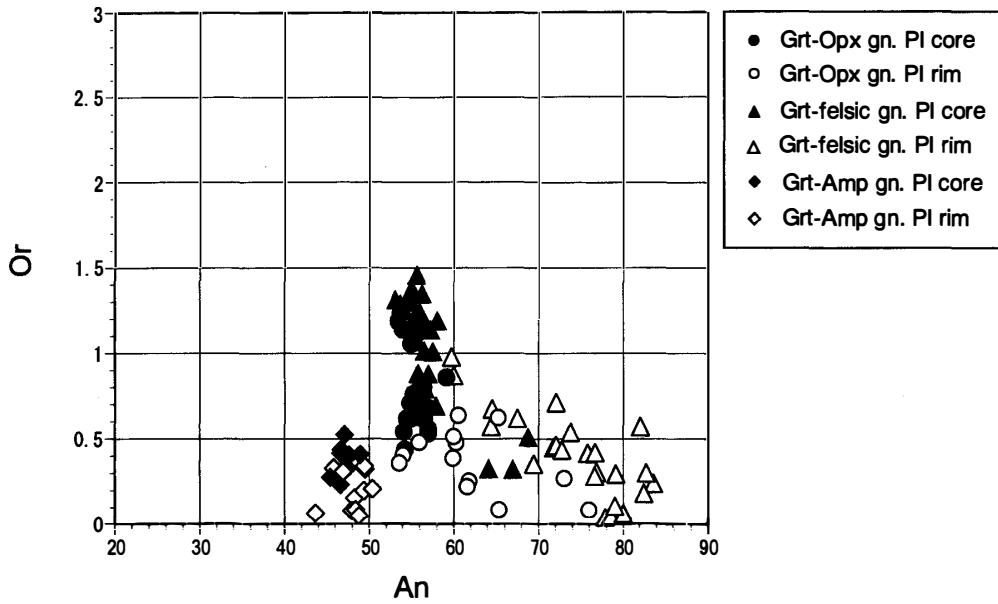
Fig. 9. Variations in Or and An content of plagioclase from garnet-orthopyroxene gneiss, garnet felsic gneiss and garnet-amphibole gneiss from Christmas Point.
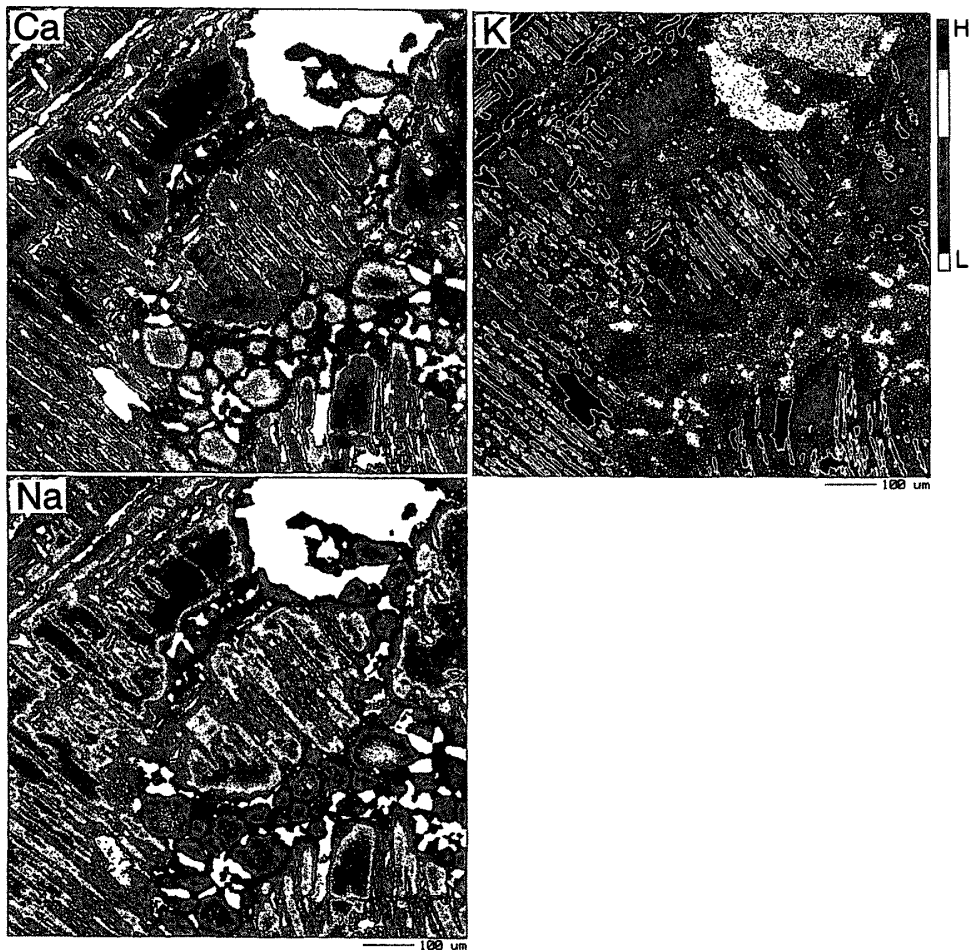
Fig. 10. Compositional color maps of plagioclase from garnet felsic gneiss (sample 9901220701). H represents higher-concentration and L is lower-concentration of each element. Note that plagioclases show reverse zoning.
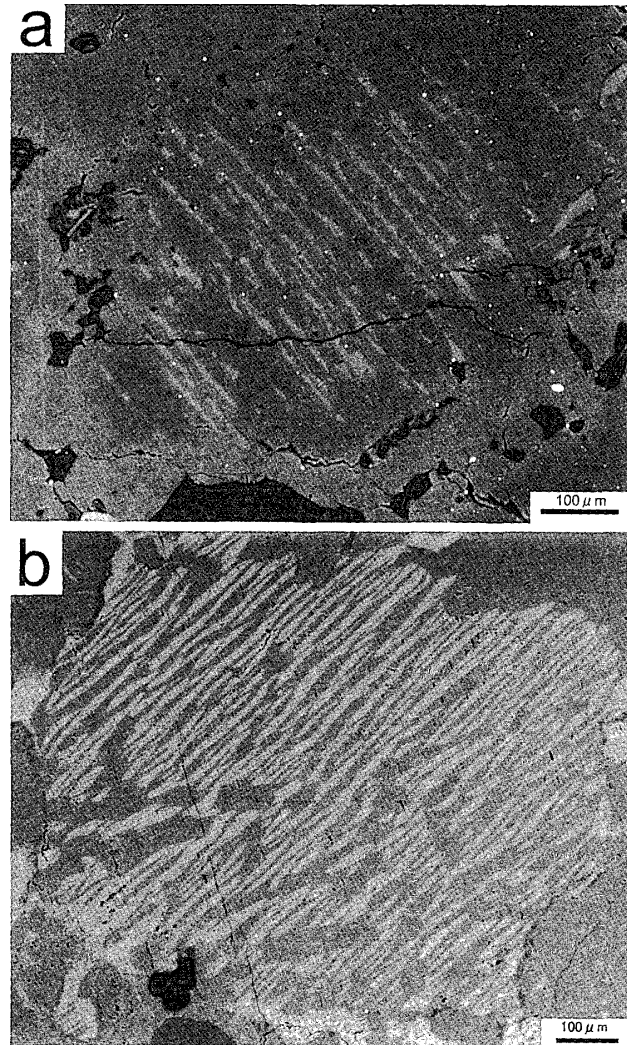
Fig. 11. *Backscattered electron images of mesoperthitic feldspar.* (a) From Christmas Point.
(b) From Howard Hills.

garnet felsic gneiss, the Ca content of the fine-grained and rounded plagioclase is relatively higher than that of the coarse-grained and antiperthitic plagioclase (Fig. 10).
3.2.4. Alkali-feldspar (mesoperthite)

Backscattered electron images (BEI) show that mesoperthite lamellae from Christmas Point are indefinite owing to diffusion (Fig. 11; BEI photograph from Howard Hills is shown for comparison). Ca contents for alkali-feldspar from the garnet-orthopyroxene gneiss and garnet felsic gneiss generally increase outward.
3.2.5. Amphibole

There are two kinds of amphibole (gedrite and cummingtonite) in the garnet-amphibole gneiss. Classification of amphiboles according to chemical composition is shown in Fig. 12. Gedrites have values of X_{Mg} = 0.64–0.68 and contain fluorine to about 0.3 wt%. The values of X_{Mg} in cummingtonite range from 0.66 to 0.72, and fluorine content is insignificant (Fig. 13).
3.2.6. Biotite

Biotite is mainly present in the garnet-amphibole gneiss, where it coexists with
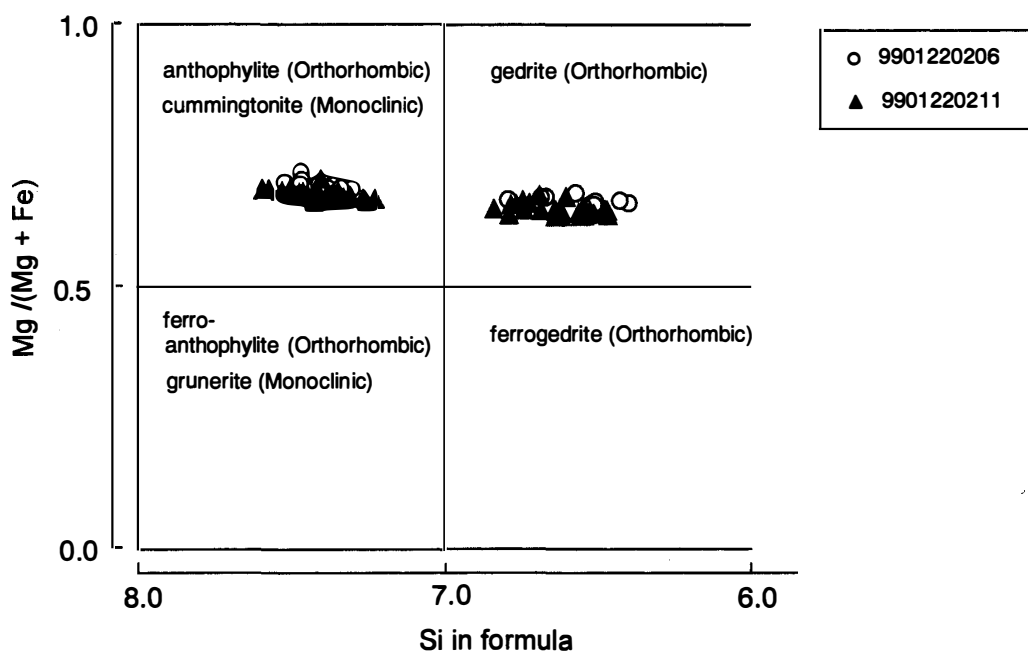
Fig. 12. Classification of the Mg-Fe-Mn-Li amphiboles (Leake et al., 1997).
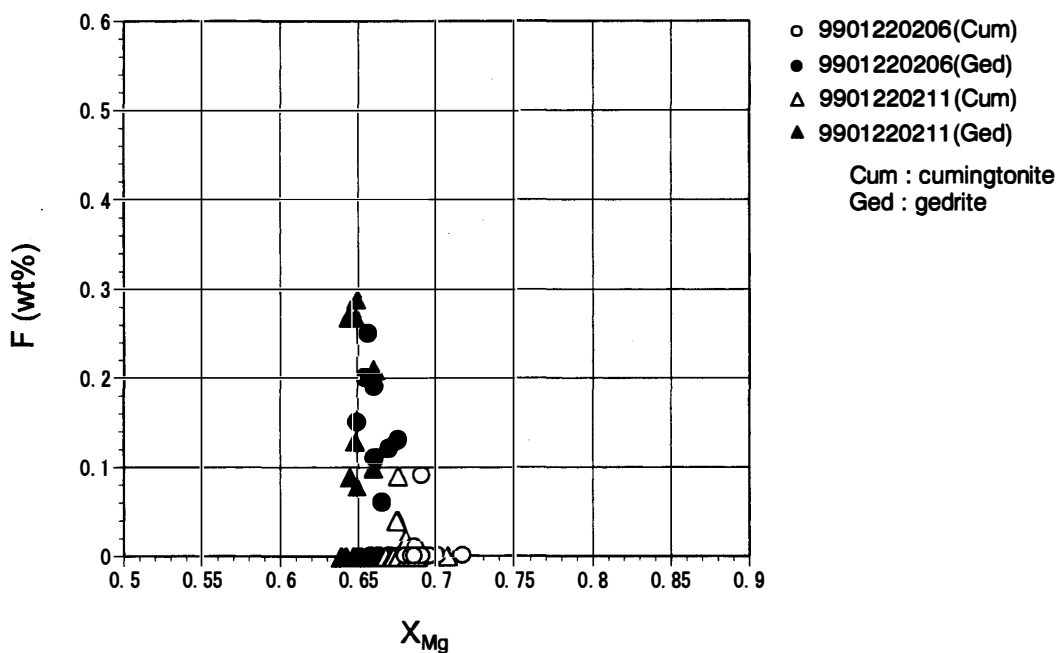
Fig. 13. Plot of F versus X_{Mg} in amphiboles from garnet-amphibole gneiss.

gedrite, cummingtonite and garnet. The X_{Mg}-F plot for biotite is shown in Fig. 14. In the garnet-amphibole gneiss, X_{Mg} and fluorine contents are 0.71–0.76 and 0–0.72 wt%, respectively. Biotite or phlogopite, regarded as a product of the UHT condition, is characterized by high fluorine contents up to 8 wt% (Motoyoshi, 1998). The biotite in the garnet-amphibole gneiss from Christmas Point, however, has lower fluorine content compared with the UHT metamorphic biotite.
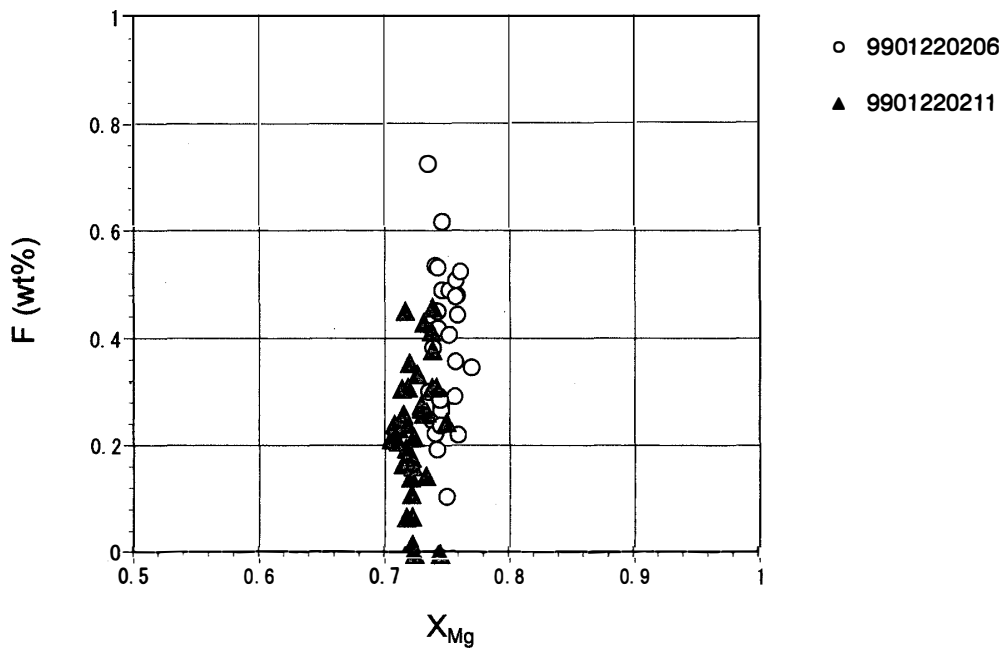
Fig. 14. Plot of F versus X_{Mg} in biotites from garnet-amphibole gneiss.

4. Discussion

4.1. Metamorphic conditions

The coexistence of orthopyroxene, sillimanite and quartz in the orthopyroxene-bearing quartz-rich granulite from Christmas Point indicates that these rocks experienced ultrahigh-temperature metamorphism. Moreover, sapphirine inclusions in the coarse crystalline sillimanite from this rock type suggest that peak metamorphic conditions were in the sapphirine+quartz stability field. This condition is the early UHT event, which occurs usually in the Napier Complex (metamorphic event M_1; *e.g.*, Sandiford, 1985; Sheraton *et al.*, 1987; Grew *et al.*, 2000). The sapphirine+quartz assemblage is reported by Grew *et al.* (2000) from Christmas Point, and implies that metamorphic conditions changed from the stability field of sapphirine+quartz [over 1030°C at 9.5 kbar (Hensen and Green, 1973) or over 1050°C at 11 kbar (Bertrand *et al.*, 1991)] during peak metamorphism to the stability field of orthopyroxene+sillimanite+quartz during retrograde metamorphism (M_2 event). Metamorphic conditions were estimated by geothermometer (Sen and Bhattachaya, 1984; Lee and Ganguly, 1988) and geobarometer (Harley 1984; corrected by Fitzsimons and Harley, 1994) using the garnet-orthopyroxene pair. The most Mg-rich garnet and the most Al-rich orthopyroxene from the garnet-orthopyroxene gneiss yield temperatures ranging from 920 to 1040°C and pressures from 8.8 to 11.5 kbar (Fig. 15). The presence of garnet lamellae in orthopyroxene, however, suggests that the reaction

high-Al orthopyroxene → lower-Al orthopyroxene+garnet,
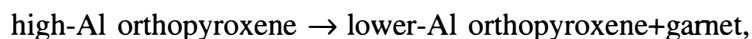
has taken place. It seems probable, therefore, that the Al content of orthopyroxene was higher at peak metamorphic conditions, and the actual metamorphic conditions were higher than those estimated using the geothermometer. Highly aluminous orthopyroxene composition is assumed to be a characteristic of ultrahigh-temperature metamorphism by
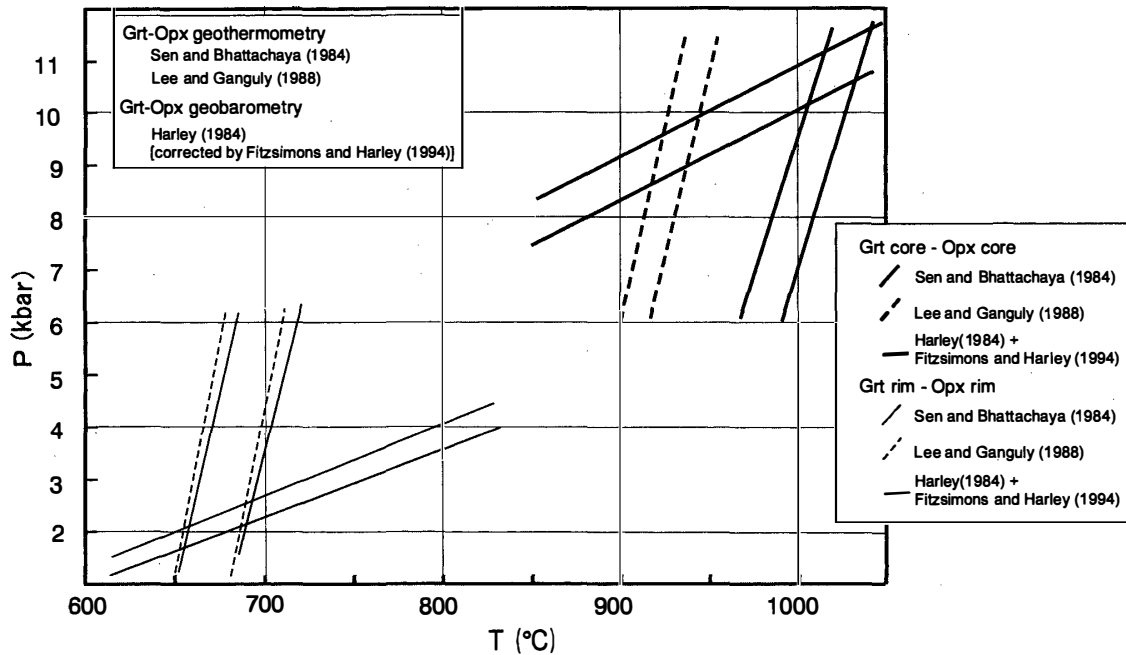
Fig. 15.   P-T conditions estimated using garnet-orthopyroxene geothermobarometry.

Hensen and Harley (1990) and Harley and Motoyoshi (2000).   The presence of Al-rich orthopyroxene in the Christmas Point rocks suggests that this region might have undergone ultrahigh-temperature metamorphism.   Orthopyroxene containing garnet exsolution lamellae has been reported from Hydrographer Island (Harley, 1985), Tonagh Island (Hokada et al., 1999a) and McIntyre Island (Kawasaki and Motoyoshi, 2000). The pair of the rim of orthopyroxene and garnet from the garnet-orthopyroxene gneiss give temperatures of 650 to 780°C, and pressures of 2 to 4 kbar (Fig. 15), which probably represents later stage metamorphism (after the M_2 event).

4.2. Retrograde metamorphism

At Christmas Point, however, most minerals or textures were formed in M_2 or after it. The following are features of the metamorphic rocks from Christmas Point: (1) garnet rims in all rock types are intergrown with quartz and have relatively high grossular composition; (2) gedrite and cummingtonite are present in the garnet-amphibole gneiss; and (3) rounded plagioclase in the garnet-orthopyroxene gneiss and garnet felsic gneiss shows reverse zoning.

Point (1) suggests that the texture formed as a result of the following reaction.

orthopyroxene+plagioclase → garnet+quartz.

In orthopyroxene-bearing quartz-rich granulite, the coexistence of orthopyroxene, sillimanite and quartz and the presence of sapphirine inclusions in sillimanite suggest the following reaction.

sapphirine+quartz → orthopyroxene+sillimanite.

These two reactions argue for an isobaric cooling path during retrograde metamorphism (Sandiford, 1985; Harley and Hensen, 1990; Harley, 1998).   In the garnet absent orthopyroxene-bearing quartz-rich granulite, a different reaction is responsible for high-Al

orthopyroxene breakdown according to the following reaction (Hensen and Essene, 1971).

high-Al orthopyroxene+quartz $\rightarrow$ lower-Al orthopyroxene+sillimanite.
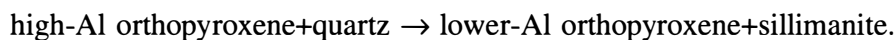
This reaction is possible because the X_{Mg} and Al zoning patterns of orthopyroxene are not similar to those of other rock types, and sillimanite is present in two crystal sizes.

Regarding point (2), cummingtonite in the garnet-amphibole gneiss was formed by the addition of water during retrograde metamorphism according to the reaction

orthopyroxene+quartz+H_2O $\rightarrow$ cummingtonite.
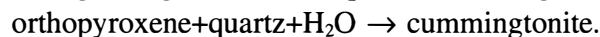
Gedrite in the garnet-amphibole gneiss formed on the margins of cummingtonites and contains some fluorine, which is effectively absent from the cummingtonite. The gedrite did not form simply as a result of retrograde metamorphism; its presence suggests the influence of a fluorine-rich fluid. Amphibole crystals containing fluorine are stable in the ultrahigh-temperature realm, whereas those that contain no fluorine form during the retrograde stage (Tsunogae *et al.*, 2000). It is necessary to examine for the presence of gedrite and cummingtonite to determine whether the formation stage differs or problem of the partitioning of the fluorine in gedrite, cummingtonite and biotite.

Regarding point (3), fine crystal size, crystal rounding (M_2 event), and reverse zoning (over An60 at the rim in the garnet-orthopyroxene and garnet felsic gneiss; Figs. 9 and 10) suggests that partial melting has taken place. Points (2) and (3) imply that the retrograde process after peak (ultrahigh-temperature; M_1) metamorphism is not simple. In addition, although compositional maps of Mg and Fe in garnet from the garnet felsic gneiss show that the zoning formed by diffusion during cooling, the structure of Ca-zoning defines domains suggesting that garnets are formed by the resorbtion and overgrowth (Fig. 6). Furthermore, exsolution of alkali feldspar into two distinct phases would take place during cooling, but these lamellae would then be obscured by diffusion during reheating.

It has been suggested that the southern part of the Napier complex was overprinted by metamorphism centered in the Rayner complex to the south (Black *et al.*, 1983; Harley, 1985; Sandiford, 1985; Sheraton *et al.*, 1987; Harley and Hensen, 1990). These studies focused on recrystallization and decompression processes interpreted to have resulted from the Rayner metamorphism and deformation. This work, however, suggests that the retrograde process took place after ultrahigh-temperature metamorphism and its retrograde process. It is thus necessary to assess whether this retrograde event took place because of Rayner metamorphism.

Acknowledgments

References

Asami, M., Suzuki, K., Adachi, M. and Grew, E.S. (1998): CHIME ages for granulites from the Napier Complex, East Antarctica. Polar Geosci., **11**, 174–201.

Bertrand, P., Ellis, D.J. and Green, D.H. (1991): The stability of sapphirine-quartz and hypersthene-sillimanite-quartz assemblages: an experimental investigation in the system $FeO-MgO-Al_2O_3-SiO_2$ under H_2O and CO_2 conditions. Contrib. Mineral. Petrol., **108**, 55–71.

Black, L.P., James, P.R. and Harley, S.L. (1983): Geochronology and geological evolution of metamorphic rocks in the Field Islands area, East Antarctica. J. Metamorph. Geol., **1**, 277–303.

Black, L.P., Fitzgerald, J.D. and Harley, S.L. (1984): Pb isotopic composition, colour, and microstructure of monazites from a polymetamorphic rock in Antarctica. Contrib. Mineral. Petrol., **85**, 141–148.

Black, L.P., Williams, I.S. and Compston, W. (1986): Four zircon ages from one rock: the history of a 3930 Ma-old granulite from Mount Sones, Antarctica. Contrib. Mineral. Petrol., **94**, 427–437.

Fitzsimons, I.C.W. and Harley, S.L. (1994): The influence of retrograde cation exchange on granulite *P-T* estimates and a convergence technique for the recovery of peak metamorphic conditions. J. Petrol., **35**, 543–576.

Grew, E.S. (1981): Surinamite, taaffeite, and beryllian sapphirine from pegmatites in granulite-facies rocks of Casey Bay, Enderby Land, Antarctica. Am. Mineral., **66**, 1022–1033.

Grew, E.S. (1998): Boron and Beryllium minerals in granulite facies pegmatites and implications of beryllium pegmatites for the origin and evolution of the Archean Napier Complex of East Antarctica. Mem. Natl Inst. Polar Res., Spec. Issue, **53**, 74–92.

Grew, E.S. and Manton, W.I. (1979): Archean rocks in Antarctica: 2.5 billion-year uranium-lead ages of pegmatites in Enderby Land, Antarctica. Science, **206**, 443–445.

Grew, E.S., Yates, M.G., Barbier, J. Shearer, C.K., Sheraton, J.W. Shiraishi, K. and Motoyoshi, Y. (2000): Granulite-facies beryllium pegmatites in the Napier Complex in Khmara and Amundsen Bays, western Enderby Land, East Antarctica. Polar Geosci., **13**, 1–40.

Harley, S.L. (1984): The solubility of alumina in orthopyroxene coexisting with garnet in $FeO-MgO-Al_2O_3-SiO_2$ and $CaO-FeO-MgO-Al_2O_3-SiO_2$. J. Petrol., **25**, 665–696.

Harley, S.L. (1985): Paragenetic and mineral-chemical relationships in orthoamphibole-bearing gneiss from Enderby Land, East Antarctica: a record of Proterozoic uplift. J. Metamorph. Geol., **3**, 179–200.

Harley, S.L. (1998): On the occurrence and characterization of ultrahigh-temperature (UHT) crustal metamorphism. What Drives Metamorphism and Metamorphic Reactions?, ed. by P.J. Treloar and P. O'Brien. London, Geol. Soc., 75–101 (Geol. Soc. London, Spec. Pub., **138**).

Harley, S.L. and Hensen, B.J. (1990): Archaean and Proterozoic high-grade terranes of East Antarctica (40–80°E): A case study of diversity in granulite facies metamorphism. High-temperature Metamorphism and Crustal Anatexis, ed. by J.R. Ashworth and M. Brown. London, Unwin Hyman, 320–370.

Harley, S.L. and Motoyoshi, Y. (2000): Al zoning orthopyroxene in a sapphirine quartzite: evidence for >1120°C UHT metamorphism in the Napier Complex, Antarctica, and implications for the entropy of sapphirine. Contrib. Mineral. Petrol., **138**, 293–307.

Hensen, B.J. and Essene, E.J. (1971): Stability of Pyrope-Quartz in the system $MgO-Al_2O_3-SiO_2$. Contrib. Mineral. Petrol., **30**, 72–83.

Hensen, B.J. and Green, D.H. (1973): Experimental study of the stability of cordierite and garnet in pelitic compositions at high pressure and temperatures. III. Synthesis of experimental data and geological applications. Contrib. Mineral. Petrol., **38**, 151–166.

Hensen, B.J. and Harley, S.L. (1990): Graphical analysis of *P-T-X* relations in granulite facies metapelites. High-temperature Metamorphism and Crustal Anatexis, ed. by J.R. Ashworth and M. Brown. London, Unwin Hyman, 19–56.

Hokada, T., Osanai, Y., Toyoshima, T., Owada, M., Tsunogae, T. and Crowe, W.A. (1999a): Petrology and metamorphism of sapphirine bearing aluminous gneiss from Tonagh Island in the Napier Complex, East Antarctica. Polar Geosci., **12**, 49–70.

Hokada, T., Ishikawa, M., Ishizuka, H., Osanai, Y. and Suzuki, S. (1999b): Alkali feldspar compositions of the Archaean Napier Complex, East Antarctica: Further evidence for 1100°C ultrahigh-temperature crustal metamorphism. Abst. 8th Int. Symp. Antarct. Earth Sci., Wellington (New Zealand), 144.

Hokada, T., Suzuki, S., Motoyoshi, Y. and Shiraishi, K. (2000): Mineral chemistry of zircon and monazite from ultrahigh-temperatture metamorphic rocks in the Napier Complex, East

Antarctica. Abst. 107th Annual Meeting of the Geological Society of Japan, 301 (in Japanese).

Kawasaki, T. and Motoyoshi, Y. (2000): High-pressure and high-temperature phase relations of an orthopyroxene granulite from McIntyre Island, Enderby Land, East Antarctica. Polar Geosci., **13**, 114–134.

Leake, B.E., Woolley, A.R., Arps, C.E.S., Brich, W.D., Gilbert, M.C., Grice, J.D., Hawthorne, F.C., Kato, A., Kish, H.J., Krivovichev, V.G., Linthout, K., Laird, J., Mandarino, J.A., Maresch, W.V., Nickel, E.H., Rock, N.M.S., Schumacher, J.C., Smith, D.C., Stephenson, N.C.N., Ungaretti, L., Whittaker, E.J.W. and Youzhi, G. (1997): Nomenclature of amphiboles: Report of the subcommittee on Amphiboles of the International Mineralogical Association, Commission on New Minerals and Mineral Names. Am. Mineral., **82**, 1019–1037.

Lee, H.Y. and Ganguly, J. (1988): Equilibrium compositions of coexisting garnet and orthopyroxene: Experimental determinations in the system $FeO-MgO-Al_2O_3-SiO_2$, and applications. J. Petrol., **29**, 93–113.

Motoyoshi, Y. (1998): Ultra-high temperature metamorphism of the Napier Complex, East Antarctica: a metamorphic perspective. J. Geol. Soc. Jpn., **104**, 794–807 (in Japanese with English abstract).

Owada, M., Osanai, Y. and Kagami, H. (1994): Isotopic equilibration age of Sm-Nd whole rock system in the Napier Complex (Tonagh Island), East Antarctica. Proc. NIPR Symp. Antarct. Geosci., **7**, 122–132.

Sandiford, M. (1985): The metamorphic evolution of granulites at Fyfe Hills; implications for Archaean crustal thickness in Enderby Land, Antarctica. J. Metamorph. Geol., **3**, 155–178.

Sen, S.K. and Bhattacharya, A. (1984): An orthopyroxene-garnet thermometer and its application to the Madras charnockites. Contrib. Mineral. Petrol., **88**, 64–71.

Sheraton, J.W., Tingey, R.J., Black, L.P., Offe, L.A. and Ellis, D.J. (1987): Geology of Enderby Land and Western Kemp Land, Antarctica. BMR Bull., **223**, 51 p.

Shiraishi, K., Ellis, D.J., Fanning, C.M., Hiroi, Y., Kagami, H. and Motoyoshi, Y. (1997): Re-examination of the metamorphic and plotolith ages of Rayner Complex, Antarctica: evidence for the Cambrian (Pan-African) regional metamorphic event. The Antarctic Region: Geological Evolution and Processes, ed. by C.A. Ricci. Siena, Terra Antarct. Publ., 79–88.

Suzuki, S., Hokada, T., Shiraishi, K. and Kagami, H. (2000): The age of UHT meramorphism at the Archaean Napier Complex, East Antarctica. Abst. 107th Annual Meeting of the Geological Society of Japan, 150 (in Japanese).

Tainosho, Y., Kagami, H., Takahashi, Y., Iizumi, S., Osanai, Y. and Tsuchiya, N. (1994): Preliminary result for the Sm-Nd whole-rock age of the metamorphic rocks from Mount Pardoe in the Napier Complex, East Antarctica. Proc. NIPR Symp. Antarct. Geosci., **7**, 115–121.

Tsunogae, T., Osanai, Y., Toyoshima, T., Owada, M., Hokada, T. and Crowe, W.A. (2000): Fluorine-rich calcic amphiboles in ultrahigh-temperature mafic granulite from Tonagh Island in the Napier Complex, East Antarctica: Preliminary report. Polar Geosci., **13**, 103–113.

Williams, I.S., Compston, W., Black, L.P. Ireland, T.R. and Foster, J.J. (1984): Unsupported radiogenic Pb in zircon: a cause of anomalously high Pb-Pb, U-Pb and Th-Pb ages. Contrib. Mineal. Petrol., **88**, 322–327.

Yoshimura, Y., Motoyoshi, Y., Grew, E.S., Miyamoto, T., Carson, C.J. and Dunkley, D.J. (2000): Ultrahigh-temperature meramorphic rocks from Howard Hills in the Napier Complex, East Antarctica. Polar Geosci., **13**, 60–85.